
[View Journal Online](#)
[View Article Online](#)

Synthesis, crystal structure with free radical scavenging activity and theoretical studies of Schiff bases derived from 1-naphthylamine, 2,6-diisopropylaniline, and substituted benzaldehyde

Segun Daniel Oladipo ^{1,2,*}, Tunde Lewis Yusuf ^{1,3,*}, Sizwe Joshua Zamisa ¹,
 Gideon Femi Tolufashe ⁴, Kolawole Ayodapo Olofinsan ⁵, Zikhona Tywabi-Ngeva ⁶
 and Nonhlangabezo Mabuba ^{3,*}

¹ School of Chemistry and Physics, University of KwaZulu-Natal, Westville campus, Private Bag X54001, Durban, 4000, South Africa
 oladipodanielsegun@gmail.com (S.D.O.), tunday@uj.ac.za (T.L.Y.), zamisas@ukzn.ac.za (S.J.Z.)

² Department of Chemical Sciences, Olabisi Onabanjo University, P.M.B. 2002, Ago-Iwoye, Nigeria

³ Department of Chemical Sciences, University of Johannesburg, Doornfontein, P.O. BOX 17011, 2028 Johannesburg, South Africa
 nmabuba@uj.ac.za (N.M.)

⁴ Department of Chemistry and Biochemistry, Faculty of Sciences, University of Porto, 4169-007 Porto, Portugal
 gideonfemitolufashe@yahoo.co.uk (G.F.T.)

⁵ Department of Biochemistry, Faculty of Natural and Applied Sciences, Nile University of Nigeria, Abuja, Nigeria
 kollyck@gmail.com (K.A.O.)

⁶ Department of Chemistry, Faculty of Sciences, Nelson Mandela University, Port Elizabeth, 6000, South Africa
 zikhona.tywabi-ngeva@mandela.ac.za (Z.T.N.)

* Corresponding author at: School of Chemistry and Physics, Westville Campus, University of KwaZulu-Natal, Private Bag X54001, Durban, 4000, South Africa.
 e-mail: tunday@uj.ac.za (T.L. Yusuf), nmabuba@uj.ac.za (N. Mabuba) and oladipodanielsegun@gmail.com (S.D. Oladipo).

RESEARCH ARTICLE



doi 10.5155/eurjchem.12.2.204-215.2088

Received: 27 January 2021

Received in revised form: 19 March 2021

Accepted: 28 March 2021

Published online: 30 June 2021

Printed: 30 June 2021

KEYWORDS

Synthesis
 Schiff bases
 Drug-likeness
 Crystal structure
 Antioxidant properties
 Density functional theory

ABSTRACT

Three Schiff bases 1-(4-chlorophenyl)-*N*-(naphthalen-1-yl)methanimine (1), 1-(4-methoxyphenyl)-*N*-(naphthalen-1-yl)methanimine (2), and 1-(4-chlorophenyl)-*N*-(2,6-diisopropylphenyl)methanimine (3) were synthesized and characterized by elemental analysis, ¹H and ¹³C NMR, FT-IR and UV-Visible spectroscopic techniques. The crystal structure of compound 3 was obtained and it revealed that the compound crystallized in a monoclinic space group *P*2₁/*n* and there exists an intermolecular hydrogen bond in a phenyl-imine form with C-H...N. Crystal data for C₁₉H₂₂ClN: *a* = 7.28280(10) Å, *b* = 9.94270(10) Å, *c* = 24.0413(2) Å, β = 97.0120(10)°, *V* = 1727.83(3) Å³, *Z* = 4, μ(Mo Kα) = 0.215 mm⁻¹, *D*_{calc} = 1.1526 g/cm³, 14038 reflections measured (12.42° ≤ 2θ ≤ 52.74°), 3448 unique (*R*_{int} = 0.0223, *R*_{sigma} = 0.0182) which were used in all calculations. The final *R*₁ was 0.0337 (*I* ≥ 2σ(*I*)) and *wR*₂ was 0.0927 (all data). The free radical scavenging activities of all three compounds were assayed using DPPH, FRAP, and OH assays. According to results obtained, compound 2 shows effective DPPH[•] (IC₅₀ = 22.69 ± 0.14 μg/mL), FRAP⁺ (IC₅₀ = 28.44 ± 0.12 μg/mL), and OH[•] (IC₅₀ = 27.97 ± 0.16 μg/mL) scavenging activities compared with compounds 1 and 3 but less than standard antioxidant compound Trolox (TRO). Additionally, theoretical calculations for the three complexes were performed by using density functional theory (DFT) calculations at the B3LYP/6-31++G(2d,2p) level in the ground state to obtain an optimized geometrical structure and to perform an electronic, molecular electronic potential surface and natural bond orbital (NBO) analysis. The geometrical calculation obtained was found to be consistent with the experimental geometry. Further analysis was conducted using the in silico technique to predict the drug likeness, molecular and ADME properties of these molecules.

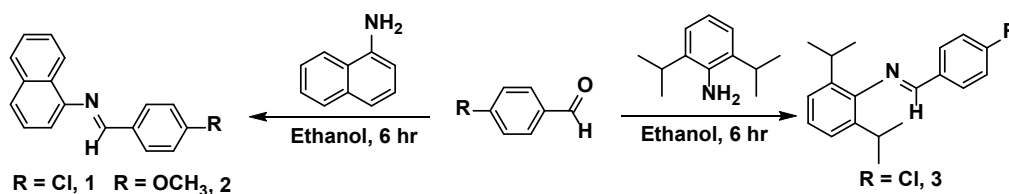
Cite this: *Eur. J. Chem.* 2021, 12(2), 204-215

Journal website: www.eurjchem.com

1. Introduction

Antioxidants are synthetic or natural compounds that delay or inhibit the oxidation process of significant macromolecules such as proteins, fats, carbohydrates, and DNA [1], and they are of great benefit to human health [2,3]. They are helpful to avert cardiovascular disease, preventing injuries associated with vessel membranes, which aids proper blood circulation in the human body [4] and to protect cells from oxidative damage, which results in ageing as well as diseases [5]. Frequently,

antioxidants are suggested at the initial stage in developing new drugs for the treatment of pathological disorders that are caused by free radicals interacting with the protein [6]. Free radicals are molecules or molecular fragments containing one or more unpaired electrons in their atomic or molecular orbitals [7]. Antioxidants help to prevent diseases caused by free radicals, and their mechanism of action has been attributed to their ability to convert free radicals to stable molecules [8,9]. However, in low concentrations, free radicals play physiological roles in cellular responses to *noxia*, such as enhancing cellular



Scheme 1. Synthesis of compounds 1-3.

signals needed for proper functioning as well as protecting living systems by killing infectious agents [10]. Research is ongoing by scientists in different disciplines to develop compounds, either synthesized or isolated from a natural source that could curb the deleterious effects of free radicals in living systems and most importantly possess antioxidant activities better than the commercially available ones.

Schiff bases have been reported to have unique biological properties such as antioxidant [11,12], antibacterial [13,14], antiglycation [15,16], antifungal [17], anticancer [18], diuretic [19] and anticonvulsant [20] activities. Aside from their biological application, they have also been used as corrosion inhibitors [21], ligands in coordination chemistry [22], and sensors [23]. They are synthesized by the condensation reaction between primary amine (R-NH₂) and an active carbonyl (aldehyde or ketone) [24], with the ones with aryl substituents relatively stable and easy to prepare than the aliphatic counterparts [25]. Schiff bases have broad-spectrum biological activities, and this could be attributed to the unique role of the imine bond (-C=N-) plays during these biological processes [26].

Recently, Bakir *et al.* [27] reported the free radical scavenging ability of Schiff bases prepared from thiocarbohydrazide, isatin, and substituted aldehydes. Their results showed that the monosubstituted products derived from thiocarbohydrazide displayed better antioxidant activity than their disubstituted counterparts which have a moiety of isatin molecule. In their report, compounds with electron-donating methoxy substituents showed better activity than others, however, none of the reported compounds displayed better antioxidant activity than the standard, gallic acid.

Herein, we report the synthesis, characterization, crystal structure, DFT calculation, and free radical scavenging properties of Schiff bases derived from 1-naphthylamine, 2,6-diisopropylaniline, and substituted aromatic aldehydes. The synthesized compounds were characterized by UV-Visible, FT-IR, and NMR spectrometry, and the purity affirmed by elemental analysis. The *in vitro* antioxidant activities were evaluated using 2,2-diphenyl-1-picrylhydrazyl, ferric reducing antioxidant power, and hydroxyl assay.

2. Experimental

2.1. Materials

All solvents (ACS reagent grade, ≥99.5 %) were obtained from Sigma-Aldrich and used as obtained without further purification. Reagents: 2,6-diisopropylaniline (97%), 1-naphthylamine (≥99%), 4-chlorobenzaldehyde (97%), and 4-methoxybenzaldehyde (98%) were obtained from Sigma Aldrich while acetic acid (≥99%) was obtained from Promark Chemicals South Africa.

2.2. Instrumentation

The melting point of the compounds was recorded using electrothermal (9100). ¹H and ¹³C NMR spectra were recorded at 25 °C on a Bruker Avance-III 400 MHz spectrometer. Both ¹H

NMR and ¹³C NMR data were recorded in either CDCl₃ referenced to the residual CDCl₃ peaks at δ 7.26 and δ 77.00 ppm. Elemental analyses were recorded on a Vario elemental EL cube CHNS analyzer. IR spectra were obtained on a PerkinElmer Universal ATR spectrum 100 FT-IR spectrometer and UV-Vis absorption spectra were recorded on Shimadzu UV-vis-NIR spectrophotometer.

2.3. Synthesis of the Schiff base ligands

To a stirring ethanolic solution of amine in a flask was added the appropriate aldehyde. To the resulting solution, 2 or 3 drops of acetic acid were added dropwise and stirring continued for 6 hr at room temperature to afford off-white precipitates. The crude product was washed with hexane three times to remove unreacted anilines, to give air-stable products and stored in a desiccator for further use.

2.3.1. Synthesis of 1-(4-chlorophenyl)-N-(naphthalen-1-yl)methanimine (1)

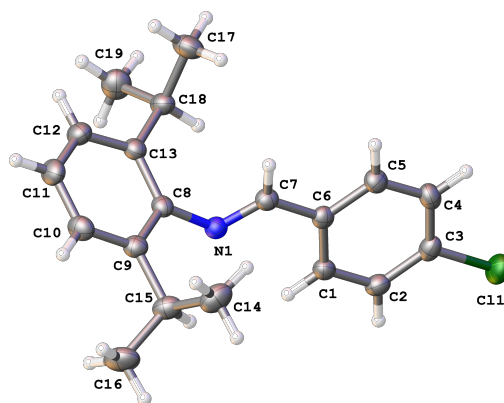
The reaction of 1-naphthylamine (1.00 g, 7 mmol) and 4-chlorobenzaldehyde (0.98 g, 7 mmol) in 20 mL of ethanol furnished Schiff base 1 as an off-white powder (Scheme 1). Color: Off white. Yield: 89 %, 1.76 g. M.p: 149-151 °C. FT-IR (ATR, ν, cm⁻¹): 3059 (w), 2878 (w), 1620 (s), 1595 (m), 1568 (m), 1264 (s), 1206 (s), 1040 (s), 801 (m), 775 (s), 501 (m). ¹H NMR (CDCl₃, 400 MHz, δ, ppm): 7.06 (d, 1H, J_{HH} = 7.24 Hz, Ar-H), 7.50 (m, 5H, J_{HH} = 7.96 Hz, Ar-H), 7.72 (d, 1H, J_{HH} = 8.24 Hz, Ar-H), 7.84 (d, 1H, J_{HH} = 6.76 Hz, Ar-H), 7.94 (d, 2H, J_{HH} = 8.32 Hz, Ar-H), 8.32 (d, 1H, J_{HH} = 9.04 Hz, Ar-H), 8.50 (s, 1H, -C=N(H)). ¹³C NMR (CDCl₃, 100 MHz, δ, ppm): 123.89, 125.84, 126.02, 126.50, 127.69, 128.81, 129.52, 130.13, 133.97, 134.93, 137.50, 148.94, 158.84. Anal. calcd for C₁₇ClH₁₂N: C, 76.84; H, 4.55; N, 5.27. Found: C, 76.25; H, 4.31; N, 5.13%. UV-Vis (CHCl₃, λ_{max}, nm): 233, 267.

2.3.2. Synthesis of 1-(4-methoxyphenyl)-N-(naphthalen-1-yl)methanimine (2)

The reaction of 1-naphthylamine (1.00 g, 7 mmol) and 4-methoxybenzaldehyde (0.95 g, 7 mmol) in 20 mL of ethanol furnished Schiff base 2 as an off-white powder (Scheme 1). Color: Off white. Yield: 91 %, 1.78 g. M.p: 145-146 °C. FT-IR (ATR, ν, cm⁻¹): 3003 (w), 2964 (w), 1600 (s), 1571 (m), 1504 (m), 1248 (s), 1248 (s), 1171 (s), 1031 (s), 837 (s), 770 (s), 516 (m). ¹H NMR (CDCl₃, 400 MHz, δ, ppm): 3.89 (s, 3H, OCH₃), 7.02 (d, 3H, J_{HH} = 8.72 Hz, Ar-H), 7.45 (t, 1H, J_{HH} = 7.80 Hz, Ar-H), 7.49 (m, 2H, Ar-H), 7.69 (d, 1H, J_{HH} = 8.24 Hz, Ar-H), 7.85 (t, 1H, J_{HH} = 6.80 Hz, Ar-H), 7.96 (d, 2H, J_{HH} = 8.68 Hz, Ar-H), 8.34 (t, 1H, J_{HH} = 6.88 Hz, Ar-H), 8.47 (s, 1H, -C=N(H)). ¹³C NMR (CDCl₃, 100 MHz, δ, ppm): 55.49, 112.74, 114.25, 124.04, 125.40, 125.61, 126.10, 126.34, 127.62, 128.89, 129.57, 130.69, 133.96, 149.66, 159.67, 162.35. Anal. calcd for C₁₈H₁₅NO: C, 82.73; H, 5.79; N, 5.36. Found: C, 82.51; H, 5.61; N, 5.16%. UV-Vis (CHCl₃, λ_{max}, nm): 232, 269.

Table 1. The summary of X-ray crystal data collection and structure refinement parameters for compound 3.

Empirical formula	C ₁₉ H ₂₂ ClN
Formula weight	299.85
Temperature (K)	150.0
Crystal system	Monoclinic
Space group	P2 ₁ /n
a (Å)	7.28280(10)
b (Å)	9.94270(10)
c (Å)	24.0413(2)
β (°)	97.0120(10)
Volume (Å ³)	1727.83(3)
Z	4
ρ _{calc} (g/cm ³)	1.1526
μ (mm ⁻¹)	0.215
F(000)	640.8
Crystal size (mm ³)	0.31 × 0.19 × 0.14
Radiation	Mo Kα (λ = 0.71073)
2θ range for data collection (°)	12.42 to 52.74
Index ranges	-9 ≤ h ≤ 7, -12 ≤ k ≤ 12, -30 ≤ l ≤ 30
Reflections collected	14038
Independent reflections	3448 [R _{int} = 0.0223, R _{sigma} = 0.0182]
Data/restraints/parameters	3448/0/194
Goodness-of-fit on F ²	1.050
Final R indexes [I ≥ 2σ (I)]	R ₁ = 0.0337, wR ₂ = 0.0856
Final R indexes [all data]	R ₁ = 0.0411, wR ₂ = 0.0927
Largest diff. peak/hole (e Å ⁻³)	0.24/-0.24

**Figure 1.** ORTEP diagram of compound 3 drawn at 50 % thermal ellipsoid probability.

2.3.3. Synthesis of 1-(4-chlorophenyl)-N-(2,6-diisopropylphenyl)methanimine (3)

The reaction of 2,6-diisopropylaniline (0.71 g, 4 mmol) and 4-chlorobenzaldehyde (0.54 g, 4 mmol) in 20 mL of ethanol furnished Schiff base **3** as an off-white powder (Scheme 1). Color: White. Yield: 84 %, 0.95 g. M.p: 120 - 121 °C. FT-IR (ATR, v, cm⁻¹): 3056 (m), 2963 (m), 1619 (s), 1594 (m), 1487 (m), 1264 (m), 1206 (s), 1087 (s), 800 (m), 774 (s). ¹H NMR (CDCl₃, 400 MHz, δ, ppm): 1.16 (d, 12H, J_{H,H} = 6.88, CH₃-CH), 2.93 (m, 2H, J_{H,H} = 6.88, CH-CH₃), 7.13 (m, 3H, Ar-H), 7.47 (d, 2H, J_{H,H} = 8.36, Ar-H), 7.45 (d, 2H, J_{H,H} = 8.40, Ar-H), 8.15 (s, 1H, -CH=N). ¹³C NMR (CDCl₃, 100 MHz, δ, ppm): 23.44, 27.99, 123.07, 124.27, 129.15, 129.73, 134.48, 137.51, 137.53, 148.98, 160.63. Anal. calcd for C₁₉H₂₂N: C, 76.11; H, 7.40; N, 4.67. Found: C, 75.91; H, 7.32; N, 4.49%. UV-Vis (CHCl₃, λ_{max}, nm): 235, 271.

2.4. Single-crystal X-ray diffraction

The crystallographic data collection of compound **3** was done on a Bruker Smart APEXII diffractometer with MoKα radiation (λ = 0.71073 Å) equipped with an Oxford Cryostream low-temperature apparatus operating at 100 K for all samples. Reflections were collected at different starting angles, and the APEXII program suite was used to index the reflections [28]. Data reduction was performed using the S_{AINT} [29] software, and the scaling and absorption corrections were applied using the S_{ADABS} [30] multi-scan technique. The structures were

solved by the direct method using the SHELXS program and refined using SHELXL program (Figure 1) [31]. Graphics of the crystal structures were drawn using Mercury software [32]. Non-hydrogen atoms were first refined isotropically and then by anisotropic refinement with the full-matrix least square method based on F² using SHELXL. All hydrogen atoms were positioned geometrically, allowed to ride on their parent atoms, and refined isotropically. The crystallographic data and structure refinement parameters for compound **3** are given in Table 1.

2.5. Density functional theory calculation

All calculations were performed using the DFT/B3LYP level of theory [33] on Gaussian 16 package [34]. The coordinates of the compounds (Figure 1) were used for geometry optimizations, using a medium-sized basis set, 6-31G(d,p). Frequency calculation revealed the compounds were fully optimized with no negative imaginary value. More accurate energies of the optimized geometries for compounds 1-3 were calculated with a double-ζ quality basis set, 6-31++G(2d,2p). Gas-phase IR spectra and TD-DFT calculation at the B3LYP/6-31++g(2d,2p) level in Chloroform was performed to retrieve the UV-vis spectrum. ¹H and ¹³C-NMR chemical shifts of the molecules in dichloromethane were computed using GIAO-SCF level [35]. HOMO and LUMO orbitals in the gas phase were also obtained from the TDDFT calculation [36].

2.6. In vitro antioxidant studies

2.6.1. 2,2-Diphenyl-1-picrylhydrazyl (DPPH) free radical scavenging assay

The antioxidant capacity of the samples was evaluated from their ability to scavenge 2,2'-diphenyl-1-picrylhydrazyl (DPPH), in a modified method described by Turkoglu *et al.* [37]. Briefly, 2 mL of each sample and standard (Trolox) was added to 2 mL 0.2 mM DPPH prepared in ethanol. The mixture was vortexed and kept under pitch-dark conditions at 25 °C for 30 min. Then, the absorbance was measured at 517 nm, and the DPPH radical mapping activity was calculated as follows:

$$\% \text{ DPPH Scavenging activity} = \frac{A_{\text{Control}} - A_{\text{Sample}}}{A_{\text{Control}}} \times 100 \quad (1)$$

where A_{control} is the absorbance of the blank solution and A_{sample} is the absorbance of the sample or standard.

2.6.2. Ferric reducing antioxidant power

The ferric reducing antioxidant properties of the chemical compounds was evaluated by adopting the method by Oyaizu [38]. 1 mL of varying concentrations of the compounds or Trolox (10-50 mM) was added to 500 μL distilled water, 100 μL 0.2 M phosphate buffer (pH = 6.6), and 100 μL 1% potassium ferricyanide [$\text{K}_3\text{Fe}(\text{CN})_6$]. The mixture was incubated at 50 °C for 20 min, followed by acidification with 100 μL trichloroacetic acid (10%). After centrifugation at 2,500 rpm for 15 min, 200 μL of the supernatant was transferred into another test tube containing 200 μL distilled water and 0.8 mL of FeCl_3 (0.1%). Finally, absorbance was measured at 700 nm in a spectrophotometer. The reductive antioxidant power was calculated thus:

$$\text{Ferric reducing antioxidant power \%} = \frac{\text{Absorbance of sample}}{\text{Absorbance of Trolox (50 mM)}} \times 100 \quad (2)$$

2.6.3. Hydroxyl radical (OH \cdot) scavenging activity

The Hydroxyl radical scavenging ability of the samples was measured using a slightly modified method of Smirnov and Cumbes [39]. Briefly, 1 mL of varying concentrations of the samples (10-50 mM) was added to 0.3 mL ferrous sulfate (8 mM), 0.25 mL hydrogen peroxide (20 mM), and 1 mL salicylic acid (3 mM). The mixture was vortexed and incubated at 37 °C for 30 min. Then, 0.45 mL of distilled water was added to each test before the solution was centrifuged at 10,000 rpm for 10 min. After that, the absorbance was read at 510 nm. The percentage hydroxyl radical scavenging activity of the samples has calculated the expression below:

$$\text{Percentage OH} \cdot \text{ scavenging (\% OH} \cdot \text{)} = \frac{A_{\text{Control}} - (A_{\text{Test}} - A_{\text{Sample}})}{A_{\text{Control}}} \times 100 \quad (3)$$

where A_{control} is the absorbance of the mixture without the test sample, A_{test} is the absorbance of the mixture with the test sample and A_{sample} is the absorbance of the sample only.

3. Results and discussion

3.1. General synthesis

The synthesis route for compounds **1-3** is shown in Scheme 1, and it was achieved by the condensation reaction between benzaldehyde derivatives (Cl and OCH_3 derivatives) and primary amines (1-naphthylamine and 2,6-diisopropylaniline) in the presence of 2 or 3 drops of acetic acid to control the pH

of the reaction. The off-white product formed is in good yield (84-91 %) and melts between 120-151 °C. The synthesized compounds showed good solubility in dichloromethane, chloroform, and toluene but were only partially soluble in other polar solvents. The spectra data, together with analytical results, conform to the structure of the synthesized compounds.

3.2. Spectroscopy studies

3.2.1. Nuclear magnetic resonance

The ^1H NMR data for compounds **1-3** were obtained in CDCl_3 and peak assignments are done using 2D NMR. The signals of methyl and diisopropyl protons for compound **3** appeared at δ 1.16 and 2.93 ppm, while the methyl protons for methoxy group ($-\text{OCH}_3$) for compound **2** appeared as a singlet at δ 3.89 ppm. The azomethine proton (NC(H)=N) for compounds **1-3** appeared as singlet between δ 8.15-8.47 ppm. The aromatic protons of the benzene and naphthalene rings appeared as multiplets, majorly duplets and triplets in the range of δ 7.01-8.34 ppm. The ^{13}C NMR spectra of compounds **1-3** showed signals ascribed to the protons of benzene and naphthalene rings between δ 112.74-149.69 ppm, and these peaks were similar to those reported in the literature [40]. The peak due to imine carbon ($-\text{C}=\text{N}$) appeared downfield at δ 158.84-160.63, and it is not exceptional to those reported in the literature [40,41] while the peak at δ 162.35 ppm in compound **2** is assigned to the carbon atom of the benzene ring attached to the methoxy group. This appeared in a far downfield region compared to other carbon atoms of the benzene ring due to the electronegative effect of the methoxy group deshielding the carbon atom [40]. The signal at δ 55.49 ppm in compound **2** is attributed to the methoxy protons ($-\text{OCH}_3$), while the ones for methyl ($\text{CH}_3\text{-CH}$) and (CH-CH_3) appeared at δ 23.44 and 27.99 ppm, respectively.

3.2.2. Fourier transform infra-red and electronic absorption spectroscopy

Three major vibrational bands were observed in the IR spectra of Schiff bases containing an aromatic ring. These are stretching vibrational bands of sp^2 C-H, sp^3 C-H, and $\nu(\text{C}=\text{N})$. For compounds **1-3**, the sp^3 C-H, sp^2 C-H, and $\nu(\text{C}=\text{N})$ vibrational bands appeared at 3003-3059, 2959-2964 and 1600-1620 cm^{-1} , respectively, and these are similar to those reported in the literature [42-44]. Other peaks such as the ones around 1504-1596 cm^{-1} could be attributed to $-\text{C}=\text{C}-$ stretching vibrational bands while the ones around 745-837 cm^{-1} may be due to out-of-plane C-H bending vibrations [40].

The electronic absorption spectra of compounds **1-3** in dichloromethane solution are given in Figure 2. The spectra of compounds **1-3** showed two major bands, one less intense absorption band on the higher energy side around 232-235 nm, and this can be assigned to the $\pi \rightarrow \pi^*$ transition due to the excitation of π -electrons in the aromatic ring. The second band appeared at 267-271 nm and can be assigned to the $\pi \rightarrow \pi^*$ transition of the imine functional group ($-\text{C}=\text{N}$) [45].

3.3. X-ray crystal structure

Suitable crystal for single-crystal X-ray diffraction analysis was obtained for compound **3** by slow evaporation of concentrated ethanol solution. The compound crystallizes in a monoclinic $P2_1/n$ space group. The asymmetric unit contains one whole of the compound (Figure 1) and it has one imine group ($\text{C7}=\text{N1}$) with the bond distance of 1.265(2) Å. There exists a non-classical hydrogen bond in a phenyl-imine form with $\text{C-H} \cdots \text{N}$. All intramolecular bond parameters are comparable with closely related compounds in the literature [46-50].

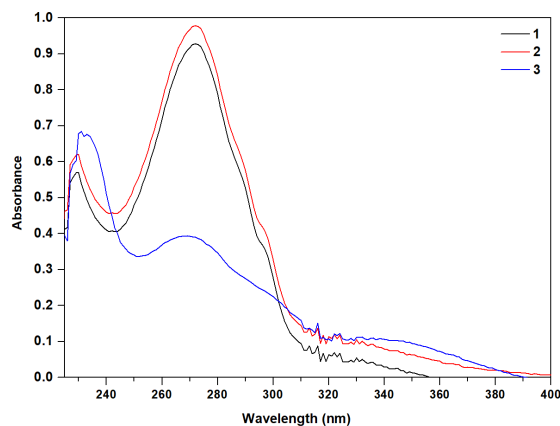


Figure 2. Electronic absorption spectra of compounds 1-3.

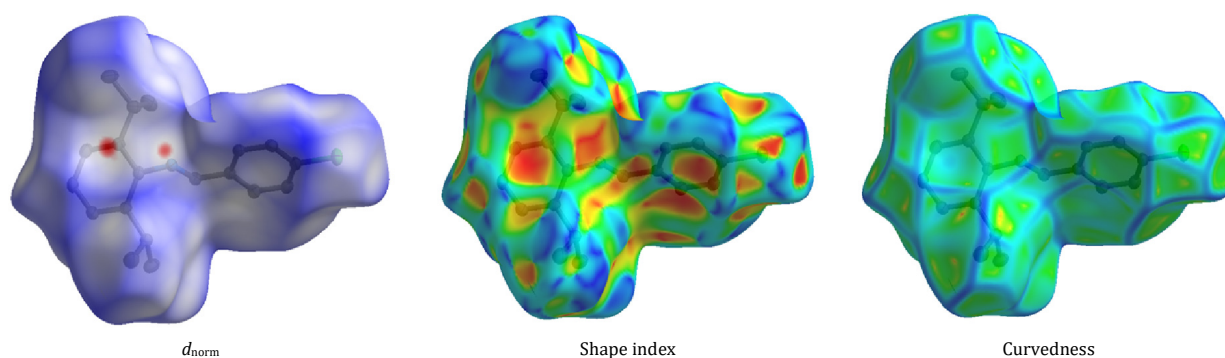


Figure 3. Hirshfeld surfaces mapped with d_{norm} (left), shape index (middle), and curvedness (right) for compound 3.

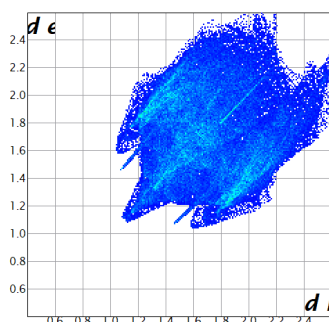


Figure 4. Fingerprint plot, where the areas of different intermolecular contacts are clearly shown.

The imine plane is significantly planar as indicated by the dihedral angle of $-4.3(2)^\circ$ for N1-C7-C6-C1 and makes an angle of 65.18° to the plane of *o,o'*-diisopropylphenyl group. There exists an intermolecular hydrogen bond in a phenyl-imine form with C-H \cdots N.

3.4. Hirshfeld surface analysis

The Hirshfeld surface is defined by the points where the contribution to electron density from the molecule inside the surface is equal to the contribution from all other molecules in a crystal [51]. Hirshfeld surface analysis is used to designate the surface characteristics of molecules as well as revealing the molecular interactions involved in their packing system. Information about existing interactions, either strong or weak, in crystal systems of molecules is described by performing Hirshfeld surface analysis [52]. Hirshfeld surfaces mapped with d_{norm} , shape index, curvedness, and 2D fingerprint plots were generated using Crystal Explorer 17.5 [53] and given in Figure

3. In the Hirshfeld surface mapped with d_{norm} for compound 3, the red region which is visible on the surface of the compound indicates hydrogen bond contacts (i.e., close contact, distance shorter than the sum of Van der Waal radii). The white region indicates the distance of contacts exactly comparable to the van der Waals separation and the blue region represents longer contacts. The full fingerprint plot depicting all the intermolecular interactions is shown in Figure 4. The major and minor intermolecular interactions with percentage contribution to total Hirshfeld surface area for compound 3 are shown in Figure 5. In the fingerprint plot, the H \cdots H hydrogen bonding interactions cover 60.0 % of the whole intermolecular interactions and this indicates that they play a major part in the molecular packing of the studied system. Other substantial interactions are C \cdots H (13.1 %) and H \cdots C (10.7 %) which appear as two wings in the fingerprint plot together with Cl \cdots H (8.2 %) and H \cdots Cl (5.3 %). The two short narrow spikes pointing towards the bottom left of the plot (Figure 4) correspond to the N \cdots H (1.0 %) and H \cdots N (0.8 %).

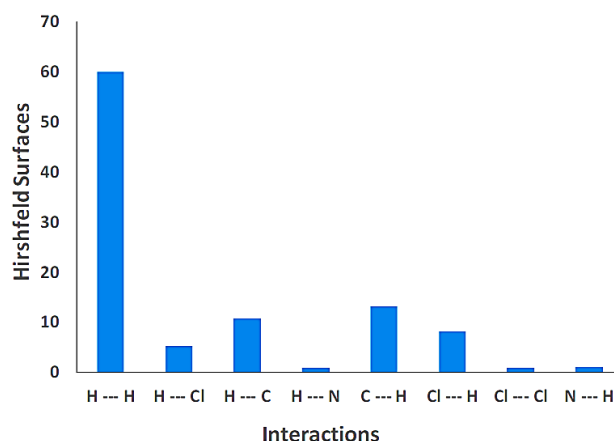


Figure 5. Relative contributions to Hirshfeld surface area for various intermolecular contacts (H...H, H...Cl, H...C, H...N, C...H, Cl...H, Cl...Cl and N...H).

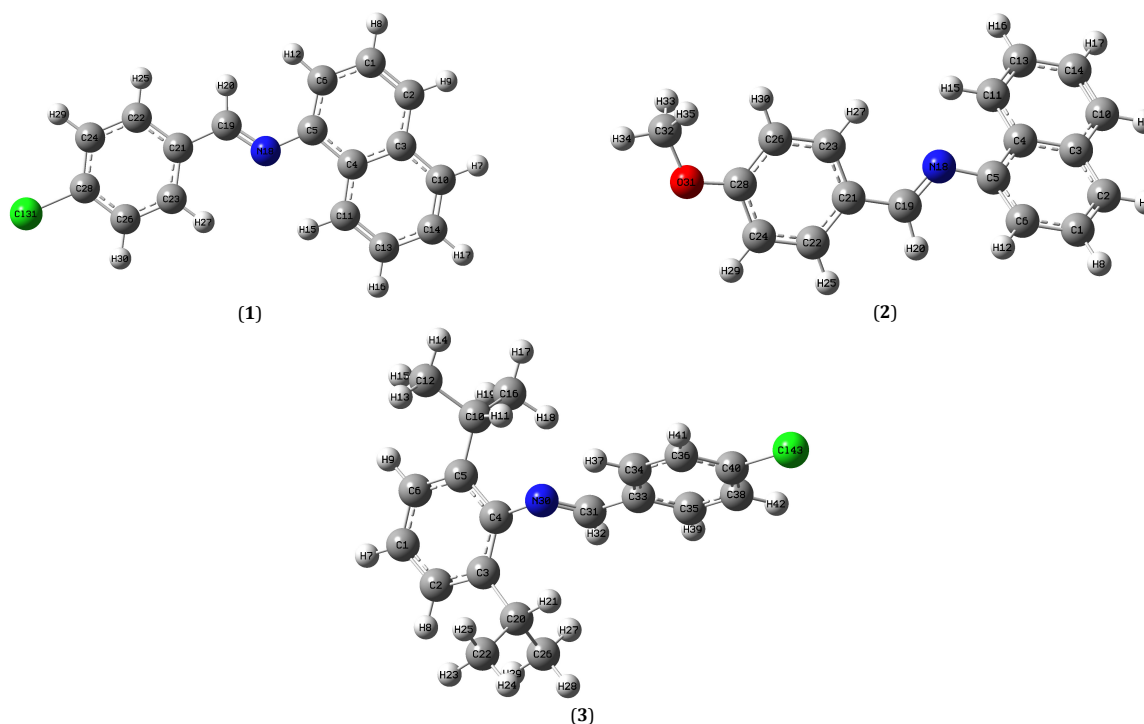


Figure 6. Optimized structures of compounds 1-3.

3.5. Density functional theory calculation

3.5.1. Frontier molecular orbital (FMO) analysis

Before the FMO, a geometry optimization of the 3D structures of compounds 1-3 (Figure 6) was optimized to obtain a stable model energy suitable for reliable further DFT analysis.

The orbitals crucial to reactivity are the highest occupied molecular orbital (HOMO) and the lowest unoccupied molecular orbital (LUMO), they are simply called frontier orbitals [54]. Most often, the filled molecular orbital having the highest energy, HOMO and to the unoccupied orbital of the lowest energy, LUMO (Table 2 and Figure 7).

Reactivity of compounds 1-3 revolves between the aromatic groups surrounding the nitrogen atom. The energy gaps are 3.47, 3.78 and 4.07 eV for compounds 1, 2, and 3, respectively. This suggests that compound 1 (small ΔE) depicts an easy transition while compounds 2 and 3 (larger ΔE) are more thermodynamically stable. Although it has been reported

that electron donor groups elevate the energy value of both HOMO and LUMO levels as noticeable for compound 3 with substituted isopropyl [55]. Thus, causing the reduction of ΔE as a result of the destabilization of the HOMO orbital. Also, the HOMO orbital energy is a frozen orbital approximation according to Koopman's theorem [56] as the minus of the ionization energy (IP) and the LUMO orbital energy is a Koopmans approximation to minus the electron affinity (EA) [57].

3.5.2. Natural bond orbitals (NBO) analysis

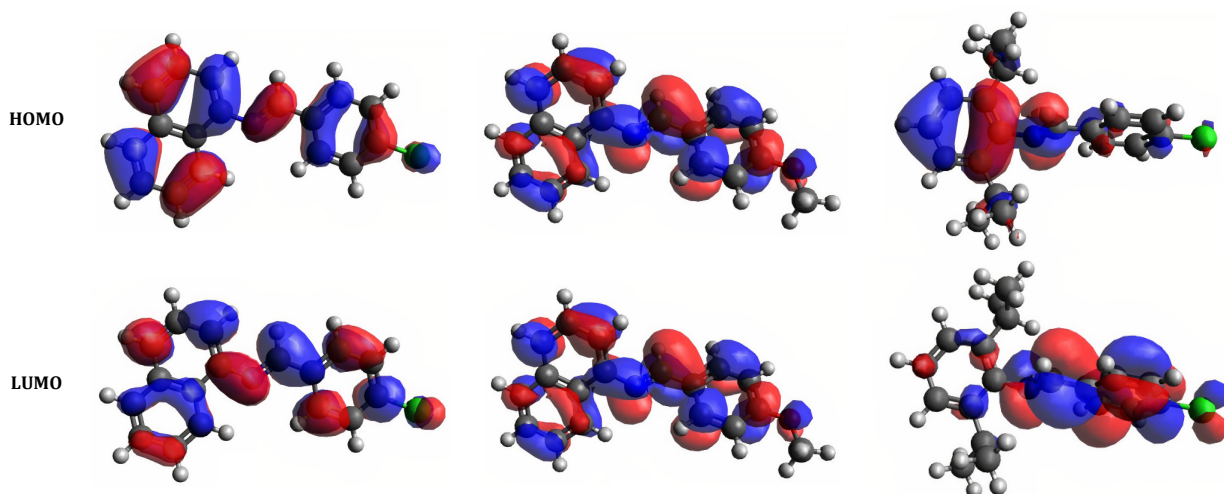
The NBO analysis results are presented in Table 3 with the calculated stabilization energies ($E^{(2)}$) resulting from the interactions between donor and acceptor atoms [donor (i) \rightarrow acceptor (j)]. This interaction can occur between occupied [for example, the lone-pair (LP)] and antibonding (BD*) orbitals, which represents the deviation of the molecule from the Lewis structure [58].

Table 2. Quantum descriptors of compounds 1-3.

Parameters	1	2	3
HOMO	-5.831	-5.578	-6.082
LUMO	-2.364	-1.803	-2.009
Energy gap (ΔE)	3.467	3.775	4.073
Ionization potential (Ip)	5.831	5.578	6.082
Electron affinity (E_A)	2.364	1.803	2.009
Dipole moment (Debye)	1.86	2.42	1.30

Table 3. NBO values of the contributing species in compounds 1-3 obtained from the second-order perturbation energies E^2 [donor (i) \rightarrow acceptor (j)].

Compound	Donor (i)	Acceptor (j)	E^2 (kcal/mol)
1	LP (1) N18	BD*(1) C19 - H20	15.18
	LP (1) Cl31	BD*(1) C26 - C28	40.88
	BD (2) C24 - C28	BD*(2) C23 - C26	33.14
	BD (1) C5 - C6	BD*(1) C10 - C14	25.34
	BD (1) C5 - C6	BD*(2) C1 - C2	17.88
2	LP (1) N18	BD*(1) C19 - H20	12.68
	LP (2) O31	BD*(2) C26 - C28	26.42
	BD (2) C1 - C2	BD*(2) C5 - C6	16.12
	BD (1) C32 - H35	BD*(1) C32 - H35	171.31
	BD (2) C26 - C28	BD*(2) C21 - C23	23.65
3	LP (1) N30	BD*(1) C31 - H32	13.40
	LP (3) Cl43	BD*(2) C38 - C40	12.67
	BD (2) C1 - C6	BD*(2) C4 - C5	20.96
	BD (2) C38 - C40	BD*(2) C34 - C36	16.96

**Figure 7.** FMO (HOMO-LUMO) surfaces of compounds 1-3.

The molecules under study comprise delocalized double, single bonds and electronegative atoms (O and N) capable of donating their lone pair of electrons for chemical bonding. Common to all, the nitrogen atom form hydrogen bonding with neighbouring atoms with significant perturbation energies of 15.18, 12.68, and 13.4 kcal/mol for compounds 1 and 2 (LP (1)N18 \rightarrow σ^* C19-H20) and 3 (LP (1)N30 \rightarrow σ^* C31-H32), respectively. In addition, intramolecular interactions resulting from π conjugation occurred in the aromatic rings. The contribution of a substituted methoxy at the para position of the phenyl of compound 2 donated more electron to the ring with E^2 of 171.31 kcal/mol between (σ (1)C32-H35 \rightarrow σ^* C32-H35).

3.5.3. Molecular electrostatic potential surface

Molecular electrostatic potential (MEP) is an approach used to visualize the charge distributions within compounds and charge related properties of compounds [59]. The most positive electrostatic potential regions are depicted in blue, red shows the areas with a smaller positive charge [60]. Besides, the regions with lone pairs atoms (N and aromatic rings) in all molecules showed negative electrostatic potential indicative of proton attraction by the concentrated electron density (red colour). However, the regions with blue color depict the positive electrostatic potential corresponds to the repulsion of

the proton by the atomic nuclei in regions where low electron density (Figure 8) [61].

3.5.4. Electronic spectra

Compounds 1-3 in the study comprise several aromatic rings with conjugated double bonds. Thus, we expect strong π - π^* transitions in the UV-Vis region having a high expansion coefficient. The electronic transitions spectra data and absorption maxima as generated in chloroform are presented in Table 4. The visible band is only seen for compound 1 around 402.21 nm (first excited state) and may be attributed to the high delocalization of π -electrons and the substituted chloride. The bands in the UV region around 381.91 and 373.61 nm for compounds 2 and 3, respectively.

3.5.5. ^1H and ^{13}C NMR chemical shifts

The ^1H and ^{13}C NMR spectra for compounds 1-3 determined by B3LYP/6-31+G(d,p) in CDCl_3 are presented in Table 5. The computational results obtained showed good agreement with the experimental. The ^1H NMR theoretical chemical shift showed a linear correlation with the experimental.

Table 4. Calculated electronic transitions for compounds 1-3.

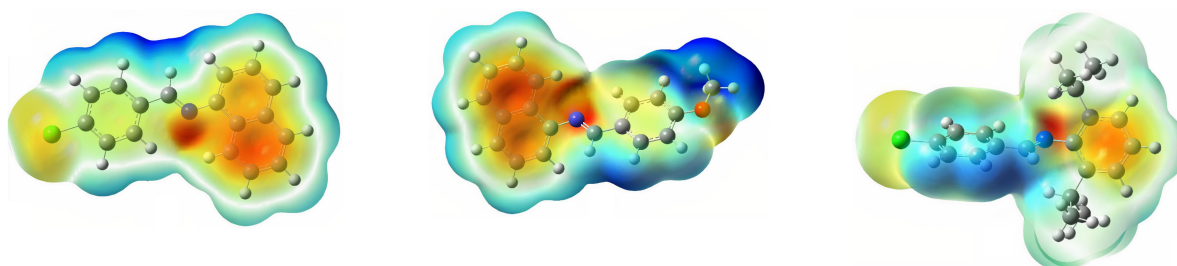
Compound	Excitations	CI expansion coefficient	Wavelength (nm)	Oscillator strength (f)
1	Excited State 1 69 -> 70	0.70357	402.21	0.6336
	Excited State 2 66 -> 70	0.70125	329.83	0.0002
	Excited State 3 68 -> 70	0.5955	314.83	0.0298
	Excited State 1 69 -> 70	0.69371	381.91	0.5453
2	Excited State 2 68 -> 70	0.49249	311.41	0.2619
	Excited State 3 67 -> 70	0.52451	300.04	0.003
	Excited State 1 80 -> 81	0.68878	373.61	0.1425
	Excited State 2 79 -> 81	0.69976	312.16	0.0064
3	Excited State 3 78 -> 81	0.65192	277.75	0.7051

Table 5. Experimental and theoretical data (DFT/B3LYP) for the ¹H and ¹³C NMR chemical shifts (ppm) for compounds 1, 2 and 3.

¹ H NMR Experimental (Theoretical), ppm			¹³ C NMR Experimental (Theoretical), ppm		
1	2	3	1	2	3
7.06 (6.96)	3.90 (3.96)	1.16 (0.93)	123.89 (120.10)	55.49 (23.22)	23.44 (22.98)
7.50 (7.05)	7.02 (7.22)	2.93 (2.56)	125.84 (122.10)	112.74 (110.11)	27.99 (28.32)
7.72 (7.53)	7.49 (7.69)	7.13 (7.23)	126.02 (124.32)	114.25 (111.13)	123.07 (122.03)
7.84 (7.77)	7.69 (7.79)	7.45 (7.56)	126.50 (124.33)	124.40 (119.69)	124.27 (122.21)
7.94 (7.79)	7.85 (7.93)	7.47 (7.61)	127.69 (126.90)	126.10 (124.86)	129.15 (126.23)
8.32 (8.02)	7.96 (8.06)	8.15 (8.30)	128.81 (126.96)	126.34 (125.20)	129.73 (128.60)
8.50 (8.22)	8.34 (8.44)		129.52 (127.20)	127.62 (125.99)	134.48 (135.19)
	8.47 (8.70)		130.13 (128.42)	128.89 (126.58)	137.51 (136.00)
			133.97 (130.92)	129.57 (126.86)	137.53 (136.42)
			134.93 (132.48)	130.69 (128.68)	148.98 (149.23)
			137.50 (134.36)	133.96 (130.99)	160.63 (159.99)
			148.94 (141.93)	146.66 (144.42)	
			158.84 (151.02)	159.67 (158.63)	
				162.35 (160.60)	

Table 6. Antioxidant potential of tested compounds 1-3 at different concentrations using DPPH, ·OH, and FRAP assays.

Compounds	DPPH assay	FRAP assay	·OH assay
	IC ₅₀ (mM)	IC ₅₀ (mM)	IC ₅₀ (mM)
1	141.32	35.55	27.96
2	89.17	28.44	27.97
3	130.24	48.28	38.84
Trolox	22.69	24.31	20.77

**Figure 8.** Contours of the molecular electrostatic potential of compounds 1-3.

The correlation values R^2 for compounds 1, 2 and 3 are 0.8359, 0.8566, and 0.7800, respectively, while for ¹³C the linear correlation values R^2 are 0.934, 0.9010, and 0.9400. The deviation ranged from 0.01-0.78 ppm. The observed deviation is consistent with similar reports.

3.6. Antioxidant studies

In this study, the antioxidant activity of the synthesized Schiff bases was evaluated *in vitro* by DPPH, Hydroxyl, and FRAP assay.

3.6.1. DPPH scavenging radical assay

DPPH assay has been used extensively to determine the antioxidant activity of compounds by quantifying their free

radical scavenging or hydrogen donor abilities [62]. DPPH has a stable free radical with an odd electron in its structure, and in the presence of antioxidants, the odd electron in DPPH paired up with proton radicals or an electron from antioxidants to form a stable diamagnetic compound [63]. During this process, the purple color of DPPH changed to yellow due to the formation of reduced DPPH-H [63]. The IC₅₀ values were used to evaluate the antioxidant activity of the compounds, and they were calculated from the % DPPH free radical scavenging ability i.e., a low IC₅₀ value is proportional to good antioxidant activity. The results are summarized in Table 6 and were compared with the antioxidant activity of Trolox (22.69 mM) which were used as standard. The IC₅₀ values of compounds 1-3 are high when compared to the ones of Trolox (Table 6), and this indicates their poor free radical scavenging ability.

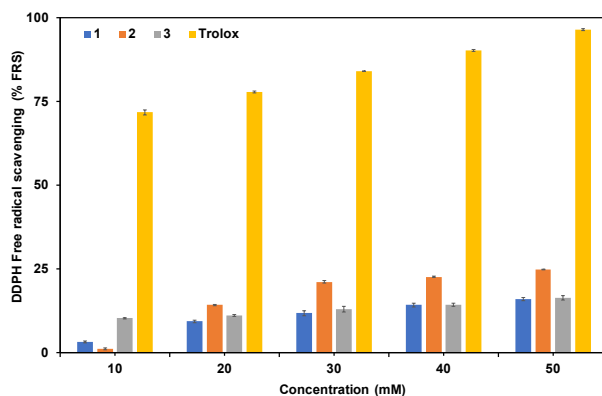


Figure 9. % Free radical scavenging vs concentration (mM) of compounds 1-3.

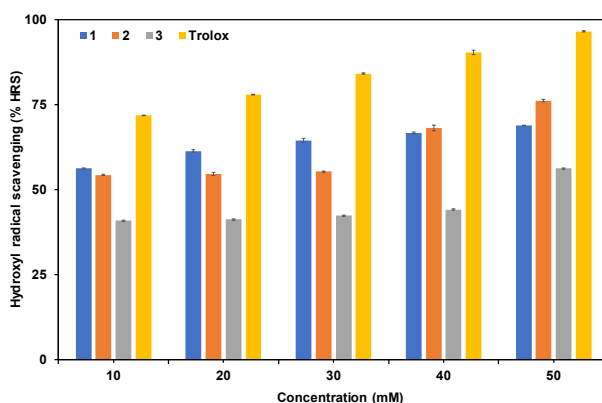


Figure 10. % Hydroxyl radical scavenging vs concentration (mM) of compounds 1-3.

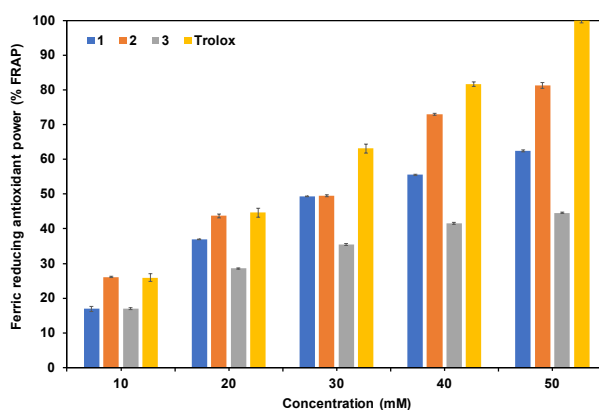


Figure 11. % Ferric reducing antioxidant power vs concentration (mM) of compounds 1-3.

Compound 2 showed the highest antioxidant activity when compared to compounds 3 and 1, and this could be attributed to the presence of electron-donating methoxy substituent in compound 2, which has been previously reported to enhance the stability of radicals, and hence antioxidant property [64]. The antioxidant activity of compounds 1-3 increases as their concentration increase, as illustrated in Figure 9. The result presented here are the mean values from three independent experiments.

3.6.2. Hydroxyl scavenging radical assay

The most reactive radical among the relative oxygen species (ROS) is the hydroxyl radical [63]. In an aqueous

solution, it has a half-life less than 1 ns and reacts very close to its site of the formation when produced *in vivo* [65]. Hydroxyl radical, when produced close to molecules such as sugar, DNA bases, amino acids, phospholipids, etc. found in living systems, cells could react with them and might change their normal physiological function [3]. The results of the OH[•] radical stabilizing potential are summarized in Table 6 and followed the order of Trolox > 2 > 1 > 3. Compound 2 displayed moderate activity, whereas compounds 1 and 3 displayed weak antioxidant activity. None of the compounds was active when compared to Trolox (standard), and their activity increases as the concentrations also increase, Figure 10.

Table 7. Predicted physicochemical and pharmacokinetic properties of compounds **1-3**.

Properties / Compounds	1	2	3	Acceptable threshold (Ro5)
Physicochemical properties				
Molecular weight (Da)	265.74	261.32	299.84	<500Da
Log P	4.68	4.08	5.65	<5
Log S (mol/L)	-5.05	-4.51	-5.70	0 → -6
TPSA (Å ²)	12.36	21.59	12.36	≤140
HBA	1	2	1	≤10
HBD	0	0	0	≤5
Rotatable bonds	2	3	4	<10
Pharmacokinetics properties				
GI absorption	High	High	Low	
BBB Permeant	Yes	Yes	No	
P-gp Substrate	No	No	No	
Log Kp (skin permeation)	-4.46	-4.90	-3.80	
Oral toxicity prediction				
LD ₅₀ (mol/kg)	2.051	2.111	2.613	
AMES toxicity	Yes	Yes	No	

3.6.3. Ferric reducing antioxidant power assay

The data obtained for the FRAP assay showed that all compounds exhibited ferric reducing antioxidant power. Compounds **1** and **2** showed almost the same antioxidant activity, while compound **3** showed the least activity (Table 6), and none of the compounds displayed better activity than Trolox. Similarly, the antioxidant activity is concentration-dependent; it increases as the concentration increases in Figure 11.

3.7. Analysis of drug likeness and pharmacokinetics of compounds 1-3

This study predicted the pharmacokinetics and pharmacological properties of compounds **1-3** using web-based analytical tools, SwissADME and pKCSM to predetermine their drug-likeness and oral bioavailability. The predicted values for significant parameters are presented in Table 7. Lipinski's Ro5 is used as a yardstick to know the violations of potential medicinal compounds from the standard and is expected to have minimal violations [66]. Parameters such as molecular weight (MW), lipophilicity (logP), tendency to be hydrogen bond acceptor (HBA) and donor (HBD), topological polar surface area (TPSA), rotatable bonds (Rots), skin permeation (Logkp), and lethal dose 50 % (LD50) were estimated and they are used to predict the extent of toxicity of these compounds when administered orally. Selected pharmacokinetic properties such as blood-brain barrier (BBB), permeant P-glycoprotein (P-gp), and gastrointestinal (GI) absorption and substrate were also predicted.

The molecular weight of compounds highly affects the rate at which drugs are absorbed into the body system. The smaller the MW of the drug, the easier they can access target biomolecules, increasing concentration at the intestinal epithelium surface, thus enhancing absorption [67]. According to Lipinski's Ro5, the acceptable MW of the active compound is ≤ 500 g/mol. The estimated values for all the compounds are within the threshold, indicating that they are bioavailable and orally active. The predicted LogP values for compounds **1** and **2** complied with Lipinski's Ro5 (< 5), while compound **3** violated it. All compounds had estimated LogS values within the standard (0 - -6 mol/L). These findings revealed that the compounds are lipophilic, thus permeate easily through the intestinal epithelium surface. These inherent attributes further established their bioavailable as well as their potential use as future drugs. The TPSA could also be used to predict the bioavailability of compounds in terms of their transportation across a lipid bilayer membrane that is closely packed, such as the gastrointestinal tract (GT) and the blood-brain barrier (BBB) [68]. TPSA considers polar atoms on the surface of compounds, such as nitrogen and oxygen, together with their added hydrogens [69]. Compounds with lower TPSA values

permeate easily through the cells when compared with those with high TPSA. The estimated TPSA values for all the compounds fall within the accepted value (≤ 140), indicating their ease to permeate through the cells, especially if they are subjected to further optimization [62].

Considering the estimations of HBAs, HBDs, and RotBs, we could predictively say compounds **1-3** are bioavailable and orally active. Rotatable bonds are single bonds, not in a ring, bound to a nonterminal heavy atom [70], and they give information about the molecular flexibility of potential drug compounds. All the compounds did not violate Lipinski's Ro5 as the estimated RotBs values fell within the acceptable threshold (RotBs < 10). Lipinski's Ro5 considers compounds with HBAs and HBDs counts of ≤5 and ≤10 to be orally active. Interestingly, all compounds had HBAs counts ≤10 with no HBDs counts, which correlate with the acceptable threshold. While developing an oral drug product, intestinal absorption must be sufficient to be successful [71]. Compounds **1** and **2** are predicted to exhibit high gastrointestinal absorption while compound **3** is low instead. These further establish compounds **1** and **2** to be bioavailable and orally active. All compounds except from compound **3** have the potential to permeate through the brain-blood barrier. The activity of P-gp in the intestine may reduce the oral bioavailability of P-gp substrate drugs [72]. All compounds are predicted not to displayed P-gp substrate properties, and this affirms their drug-likeness properties. The rate at which the compounds penetrate the skin is in the order of compounds **2** > **1** > **3**.

4. Conclusion

Schiff bases have been traditionally studied for biological properties for several decades. This study further stretches the limits of the potential application of Schiff bases and their application as antioxidant. The study reports the synthesis of three Schiff base compounds and elucidated using NMR, FT-IR, UV-Visible spectroscopic techniques and single-crystal X-ray diffraction measurements. The free radical scavenging properties of all three compounds were studied using DPPH, FRAP, and OH assays. Compared with the historical experimental work on this class of compounds, theoretical studies of correlating structural and spectroscopic properties have just begun to emerge. The DFT calculations employed the B3LYP function with 6-31+G(d,p) basis set for all atoms to obtain an optimized geometrical structure, electronic and natural bond orbital (NBO) analysis. Several theoretical parameters such as frontier molecular orbital, electrostatic potential analysis, nuclear magnetic resonance, Hirshfeld Surface Analysis, drug likeness, and pharmacokinetics analysis of the compounds are reported to further give a theoretical insight into the properties of the compounds.

Acknowledgements

The authors would like to thank the College of Agriculture, Science, and Engineering, the University of Kwazulu-Natal and the Center for High-Performance Computing (CHPC), South Africa for providing computational resources. Dr. Tunde Lewis Yusuf is grateful to Faculty of Science (FRC/URC) postdoctoral support, University of Johannesburg, South Africa.

Supporting information

CCDC-2058763 contains the supplementary crystallographic data for this paper. These data can be obtained free of charge via <https://www.ccdc.cam.ac.uk/structures/>, or by emailing data_request@ccdc.cam.ac.uk, or by contacting The Cambridge Crystallographic Data Centre, 12 Union Road, Cambridge CB2 1EZ, UK; fax: +44(0)1223-336033.

Disclosure statement

Conflict of interests: The authors declare that they have no conflict of interest.

Author contributions: All authors contributed equally to this work.

Ethical approval: All ethical guidelines have been adhered.

Sample availability: Samples of the compounds are available from the author.

ORCID

Segun Daniel Oladipo

 <https://orcid.org/0000-0003-2489-1752>

Tunde Lewis Yusuf

 <https://orcid.org/0000-0003-3419-9516>

Sizwe Joshua Zamisa

 <https://orcid.org/0000-0003-1968-381X>

Gideon Femi Tolufashe

 <https://orcid.org/0000-0002-0852-9756>

Kolawole Ayodapo Olofinas

 <https://orcid.org/0000-0002-2987-0996>

Zikhona Tywabi-Ngeva

 <https://orcid.org/0000-0002-5290-6942>

Nonhlangabezo Mabuba

 <https://orcid.org/0000-0003-0209-7451>

References

- Kerr, M. E.; Bender, C. M.; Monti, E. J. *Heart Lung* **1996**, *25* (3), 200–209.
- Oladipo, S. D.; Omondi, B.; Mocktar, C. *Polyhedron* **2019**, *170*, 712–722.
- Valko, M.; Leibfritz, D.; Moncol, J.; Cronin, M. T. D.; Mazur, M.; Telser, J. *Int. J. Biochem. Cell Biol.* **2007**, *39* (1), 44–84.
- Hertog, M. G.; Feskens, E. J.; Hollman, P. C.; Katan, M. B.; Kromhout, D. *Lancet* **1993**, *342* (8878), 1007–1011.
- Aziz, A. N.; Taha, M.; Ismail, N. H.; Anouar, E. H.; Yousuf, S.; Jamil, W.; Awang, K.; Ahmat, N.; Khan, K. M.; Kashif, S. M. *Molecules* **2014**, *19* (6), 8414–8433.
- Kostova, I.; Saso, L. *Curr. Med. Chem.* **2013**, *20* (36), 4609–4632.
- Halliwell, B.; Gutteridge, J. M. C. *Free Radicals in Biology and Medicine*, 5th ed.; Oxford University Press: London, England, 2015.
- Oladipo, S. D.; Omondi, B.; Mocktar, C. *Appl. Organomet. Chem.* **2020**, *34* (5), e5610.
- Riley, P. A. *Int. J. Radiat. Biol.* **1994**, *65* (1), 27–33.
- Valko, M.; Rhodes, C. J.; Moncol, J.; Izakovic, M.; Mazur, M. *Chem. Biol. Interact.* **2006**, *160* (1), 1–40.
- Gacche, R. N.; Gond, D. S.; Dhole, N. A.; Dawane, B. S. *J. Enzyme Inhib. Med. Chem.* **2006**, *21* (2), 157–161.
- Khan, K. M.; Khan, M.; Ambreen, N.; Rahim, F.; Muhammad, B.; Ali, S.; Haider, S. M.; Perveen, S.; Choudhary, M. *J. Pharm. Res.* **2011**, *4* (10), 3402–3404.
- Yusuf, T. L.; Oladipo, S. D.; Olagboye, S. A.; Zamisa, S. J.; Tolufashe, G. F. *J. Mol. Struct.* **2020**, *1222* (128857), 128857.
- Mohapatra, R. K.; Das, P. K.; Pradhan, M. K.; Maihub, A. A.; El-ajaily, M. M. *J. Iran. Chem. Soc.* **2018**, *15* (10), 2193–2227.
- Khan, K. M.; Khan, M.; Ali, M.; Taha, M.; Rasheed, S.; Perveen, S.; Choudhary, M. I. *Bioorg. Med. Chem.* **2009**, *17* (22), 7795–7801.
- Khan, K. M.; Rahim, F.; Ambreen, N.; Taha, M.; Khan, M.; Jahan, H.; Najeebullah; Shaikh, A.; Iqbal, S.; Perveen, S.; Choudhary, M. I. *Med. Chem.* **2013**, *9* (4), 588–595.
- Sundriyal, S.; Sharma, R. K.; Jain, R. *Curr. Med. Chem.* **2006**, *13* (11), 1321–1335.
- Shukla, S.; Srivastava, R. S.; Shrivastava, S. K.; Sodhi, A.; Kumar, P. *Med. Chem. Res.* **2013**, *22* (4), 1604–1617.
- Mishra, P.; Gupta, P.; Shakya, A. K.; Shukla, R.; Srimal, R. *Indian J. Physiol. Pharmacol.* **1995**, *39* (1), 169–172.
- Jain, J.; Srivastava, R.; Aggarwal, N.; Sinha, R. *Cent. Nerv. Syst. Agents Med. Chem.* **2007**, *7* (3), 200–204.
- Shetty, P. *Chem. Eng. Commun.* **2020**, *207* (7), 985–1029.
- Olagboye, S. A.; Yusuf, T. L.; Oladipo, S. D.; Zamisa, S. J. *Z. Krist. - New Cryst. Struct.* **2020**, *235* (3), 689–692.
- Berhanu, A. L.; Gaurav; Mohiuddin, I.; Malik, A. K.; Aulakh, J. S.; Kumar, V.; Kim, K.-H. *Trends Analyt. Chem.* **2019**, *116*, 74–91.
- Olagboye, S. A.; Yusuf, T. L.; Oladipo, S. D.; Zamisa, S. J. *Z. Krist. - New Cryst. Struct.* **2020**, *235* (4), 833–836.
- Hine, J.; Yeh, C. Y. *J. Am. Chem. Soc.* **1967**, *89* (11), 2669–2676.
- Mermer, A.; Demirbas, N.; Uslu, H.; Demirbas, A.; Ceylan, S.; Sirin, Y. *J. Mol. Struct.* **2019**, *1181*, 412–422.
- Bakur, T. K.; Lawag, J. B. *Res. Chem. Intermed.* **2020**, *46* (5), 2541–2557.
- APEX2 Bruker, Bruker AXS Inc., Wisconsin, Madison, USA, 2004.
- SAINT-Plus, Bruker AXS Inc., Wisconsin, Madison, USA, 2004.
- SADABS, Bruker AXS Inc., Wisconsin, Madison, USA, 2004.
- Sheldrick, G. M. *Acta Crystallogr. A* **2008**, *64* (1), 112–122.
- Macrae, C. F.; Bruno, I. J.; Chisholm, J. A.; Edgington, P. R.; McCabe, P.; Pidcock, E.; Rodriguez-Monge, L.; Taylor, R.; van de Streek, J.; Wood, P. A. *J. Appl. Crystallogr.* **2008**, *41* (2), 466–470.
- Becke, A. D. *Phys. Rev. A Gen. Phys.* **1988**, *38* (6), 3098–3100.
- Long, F.; Zhang, X.; Cao, X.; Zhai, Q.; Song, Y.; Wang, F.; Jiang, J.; Xu, J. *Fuel Process. Technol.* **2020**, *200* (106312), 106312.
- Buehl, M.; Thiel, W.; Fleischer, U.; Kutzelnigg, W. *J. Phys. Chem.* **1995**, *99* (12), 4000–4007.
- Fabian, J. *Dyes Pigm.* **2010**, *84* (1), 36–53.
- Turkoglu, A.; Duru, M. E.; Mercan, N.; Kivrak, I.; Gezer, K. *Food Chem.* **2007**, *101* (1), 267–273.
- Oyaizu, M. *Jpn. J. Nutr. Diet.* **1986**, *44* (6), 307–315.
- Smirnov, N.; Cumbes, Q. J. *Phytochemistry* **1989**, *28* (4), 1057–1060.
- Elemike, E. E.; Nwankwo, H. U.; Onwudiwe, D. C. *J. Mol. Struct.* **2018**, *1155*, 123–132.
- Elemike, E. E.; Onwudiwe, D. C.; Nwankwo, H. U.; Hosten, E. C. *J. Mol. Struct.* **2017**, *1136*, 253–262.
- Al Zoubi, W.; Al-Hamdani, A. A. S.; Ahmed, S. D.; Ko, Y. G. *J. Phys. Org. Chem.* **2018**, *31* (2), e3752.
- Arifuzzaman, M.; Karim, M. R.; Siddiquee, T. A.; Mirza, A. H.; Ali, M. A. *Int. J. Org. Chem. (Irvine)* **2013**, *03* (01), 81–86.
- Naeimi, H.; Safari, J.; Heidarneshad, A. *Dyes Pigm.* **2007**, *73* (2), 251–253.
- Issa, R. M.; Khedr, A. M.; Rizk, H. J. *Chin. Chem. Soc.* **2008**, *55* (4), 875–884.
- Oladipo, S. D.; Omondi, B. *Transit. Met. Chem.* **2020**, *45* (6), 391–402.
- Oladipo, S. D.; Mocktar, C.; Omondi, B. *Arab. J. Chem.* **2020**, *13* (8), 6379–6394.
- Khosravi, I.; Hosseini, F.; Khorshidifard, M.; Sahihi, M.; Rudbari, H. A. *J. Mol. Struct.* **2016**, *1119*, 373–384.
- Aldoshin, S. M.; Chuev, I. I.; Kozina, O. A. *Mol. Cryst. Liq. Cryst.* **1995**, *264* (1), 215–226.
- Ferguson, G.; Glidewell, C.; Low, J. N.; Skakle, J. M. S.; Wardell, J. L. *Acta Crystallogr. C* **2005**, *61* (Pt 7), o445–9.
- Selvaganapathi, P.; Thirumarani, S.; Ciattini, S. J. *J. Mol. Struct.* **2017**, *1148*, 547–556.
- Mudsainiyan, R. K.; Pandey, S. K. *Z. Anorg. Allg. Chem.* **2017**, *643* (20), 1245–1252.
- Spackman, M. A.; Jayatilaka, D. *CrystEngComm* **2009**, *11* (1), 19–32.
- Fleming, I. *Molecular orbitals and organic chemical reactions*; ISBN: 978-0-470-74658-5, John Wiley & Sons, 2011.
- Aicha, Y. A.; Bouzzine, S. I. M.; Zair, T.; Bouachrine, M.; Hamidi, M.; Salgado-Morán, G.; Tagle, R. R.; Mendoza-Huizar, L. H. *J. Chil. Chem. Soc.* **2017**, *62* (3), 3637–3646.
- Vargas, R.; Garza, J.; Cedillo, A. J. *J. Phys. Chem. A* **2005**, *109* (39), 8880–8892.
- Borghini, G.; Ferretti, A.; Nguyen, N. L.; Dabo, I.; Marzari, N. *Phys. Rev. B Condens. Matter Mater. Phys.* **2014**, *90* (7), 075135.
- Glendening, E.; Reed, A.; Carpenter, J.; Weinhold, F. NBO Version 3.1, TCI, University of Wisconsin, Madison, 1998.
- Vetrivel, R.; Deka, R. C.; Chatterjee, A.; Kubo, M.; Broclawik, E.; Miyamoto, A. *Studies on the Molecular Electrostatic Potential inside the Microporous Material and Its Relevance to Their Catalytic Activity. In Theoretical and Computational Chemistry*; Elsevier, 1996; pp 509–541.
- Silva, P. J.; Ramos, M. J. *J. Org. Chem.* **2009**, *74* (16), 6120–6129.

- [61]. Ophardt, C. E.; Ophardt, C. E. *Virtual Chembook: Elmhurst College*; Elmhurst College, 2003.
- [62]. Oladipo, S. D.; Olotu, F. A.; Soliman, M.; Mocktar, C.; Omondi, B. J. *Mol. Struct.* **2020**, *1219* (128553), 128553.
- [63]. Vartale, S. P.; Halikar, N. K.; Pawar, Y. D.; Tawde, K. V. *Arab. J. Chem.* **2016**, *9*, S1117–S1124.
- [64]. Pakravan, P.; Kashanian, S.; Khodaei, M. M.; Harding, F. J. *Pharmacol. Rep.* **2013**, *65* (2), 313–335.
- [65]. Pastor, N.; Weinstein, H.; Jamison, E.; Brenowitz, M. J. *Mol. Biol.* **2000**, *304* (1), 55–68.
- [66]. Lipinski, C. A. *J. Pharmacol. Toxicol. Methods* **2000**, *44* (1), 235–249.
- [67]. Olotu, F. A.; Munsamy, G.; Soliman, M. E. S. *Comput. Struct. Biotechnol. J.* **2018**, *16*, 573–586.
- [68]. Shityakov, S.; Neuhaus, W.; Dandekar, T.; Förster, C. *Int. J. Comput. Biol. Drug Des.* **2013**, *6* (1–2), 146–156.
- [69]. Prasanna, S.; Doerksen, R. J. *Curr. Med. Chem.* **2009**, *16* (1), 21–41.
- [70]. Veber, D. F.; Johnson, S. R.; Cheng, H.-Y.; Smith, B. R.; Ward, K. W.; Kopple, K. D. *J. Med. Chem.* **2002**, *45* (12), 2615–2623.
- [71]. Sjögren, E.; Westergren, J.; Grant, I.; Hanisch, G.; Lindfors, L.; Lennernäs, H.; Abrahamsson, B.; Tannergren, C. *Eur. J. Pharm. Sci.* **2013**, *49* (4), 679–698.
- [72]. Cornaire, G.; Woodley, J.; Hermann, P.; Cloarec, A.; Arellano, C.; Houin, G. *Int. J. Pharm.* **2004**, *278* (1), 119–131.



Copyright © 2021 by Authors. This work is published and licensed by Atlanta Publishing House LLC, Atlanta, GA, USA. The full terms of this license are available at <http://www.eurjchem.com/index.php/eurjchem/pages/view/terms> and incorporate the Creative Commons Attribution-Non Commercial (CC BY NC) (International, v4.0) License (<http://creativecommons.org/licenses/by-nc/4.0>). By accessing the work, you hereby accept the Terms. This is an open access article distributed under the terms and conditions of the CC BY NC License, which permits unrestricted non-commercial use, distribution, and reproduction in any medium, provided the original work is properly cited without any further permission from Atlanta Publishing House LLC (European Journal of Chemistry). No use, distribution or reproduction is permitted which does not comply with these terms. Permissions for commercial use of this work beyond the scope of the License (<http://www.eurjchem.com/index.php/eurjchem/pages/view/terms>) are administered by Atlanta Publishing House LLC (European Journal of Chemistry).